RESEARCH PAPER

Effect of Threaded Pin Tool for Friction Stir Welding of AA6061-T6 at Varying Traverse Speeds: Torque and Force Analysis

Abhijit Banik[1] · John Deb Barma[1] · Subhash Chandra Saha[1]

Abstract

Friction stir welding (FSW) of 6-mm-thick AA 6061-T6 plates for taper threaded tool were studied in this investigation in terms of torque and different forces. A plain taper tool in addition to threaded tool is also incorporated in the study to analyze the effectiveness of threads. Welding was conducted at a constant rotational speed of 1100 RPM and varying traverse speeds between 45 and 135 mm/min. The distribution of torque, Z-force and X-force generated during the FSW process discloses a substantial knowledge about the weld formation. The torque and forces increase with the increase in traverse speed for both the tools where higher values were attained by taper threaded tool. The macrostructure reveals a sudden increase in thickness of shoulder induced region and nugget area, followed by a gradual decrease for both of the tools with traverse speed. Comparatively larger shoulder induced region and weld nugget are obtained for taper threaded tool. The maximum values of these entities were attained at 75 mm/min for taper threaded tool, and a difference of 0.13 mm and 7.52 mm², respectively, was obtained with taper tool. Finer grains with an average diameter of 5.82 μm are obtained for taper threaded tool and 8.68 μm for taper tool. Maximum tensile strength was obtained for taper threaded tool with a joint efficiency of 70.96% and 60.32% for taper tool. A mixed mode of failure is observed at a higher traverse speed for taper tool, whereas all welds for taper threaded tool exhibit ductile fracture.

Keywords Friction stir welding · Tool design · Torque · Z-force · X-force · Microstructure

1 Introduction

Friction stir welding (FSW) process was developed at TWI in 1991 to weld aluminum alloys which are difficult to weld by conventional fusion welding process (Thomas et al. 1991). The ability of this process to accomplish the joining operation at the solid state of the workpiece gives it immense flexibility over conventional fusion welding processes. The joining is done by a non-consumable rotating tool with a pin which plunges into the joining line of the workpiece followed by a traverse movement along the joining line. In this process, heat is generated at the tool–workpiece interface by friction and workpiece deformation (Mishra and Ma 2005).

Different forces and torque commonly known as spindle torque are generated at the tool–workpiece interface during this process due to material deformation and flow (Fig. 1). Spindle torque is an important requirement in FSW which is generated due to the rotational movement of the machine spindle attached with the tool. It dictates the deformation of the workpiece by the FSW tool and the state of the deformed material. A vertically downward force (Z-force) is applied by the tool shoulder to the workpiece during the joining process. This provides workpiece deformation and effective consolidation of displaced, deformed material by tool shoulder to the trailing side of the tool. Increased Z-force further provides enhanced frictional heat. During the traverse movement of the tool, the deformed material passes across the tool pin from the advancing side to the retreating side over the pin surface due to tool rotation exerting a resistance force on the tool pin known as X-force (Banik et al. 2018; Mishra and Ma 2005). The distribution of all these forces and spindle torque depends on a complex combination of
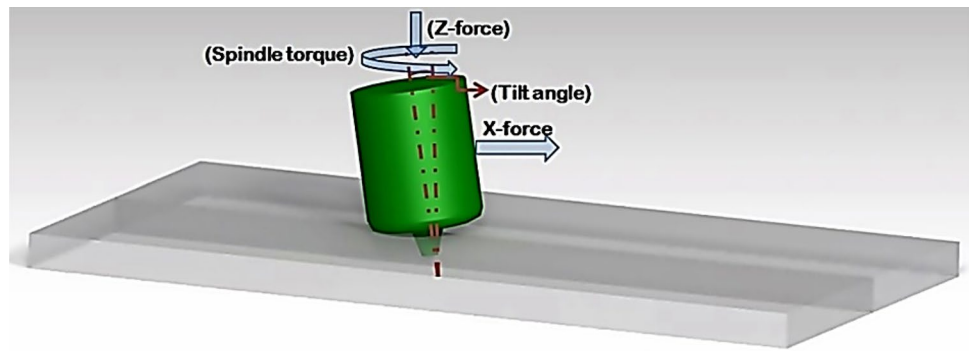
✉ Abhijit Banik
    abanikme.sch@nita.ac.in; jitniknita2016@gmail.com

    John Deb Barma
    debbarma_john@rediffmail.com

    Subhash Chandra Saha
    subashchandrasaha@yahoo.in

1   Department of Mechanical Engineering, NIT Agartala,
    AGARTALA 799046, India

Fig. 1 Schematic diagram of spindle torque and different forces generated during FSW

different process parameters (tool design, rotational speed, tool traverse speed, tilt angle, workpiece material, cooling strategy, etc.) which finally contributes to weld quality. Analysis of these entities (spindle torque, X-force and Z-force) provides an opportunity of online weld quality monitoring and controlling, thereby reducing the post-weld quality testing, cost and time. Development of a detailed idea of these entities in relation to FSW will further add to the knowledge of industry personnel in shop floor in real time providing more flexibility. With the advancement of electronics and instrumentation facilities for measurement (Santochi and Dini 1998; Teti et al. 2010) researchers from different fields have shown their interest to explore a better understanding of this process. Yang et al. developed a monitoring algorithm by filtering the applied vertical force for detection of a gap in the nugget (Yang et al. 2008). Kumar (2016) in their study reported reductions of X-force and vertical force for ultrasonic-assisted friction stir welding and inferred that such reduction was assisted by ultrasonic vibration.

With the development of the FSW process, at the same time, attempts for development of newer FSW tool design and their affectivity analysis are continued. The tool design affects the material stirring action and heat generation. Tool pin profile has an important impact on the torque and force generation. Elangovan et al. in their study attempted to establish the effect of vertically applied load on weld quality with variation in tool pin design. They found that with the moderate amount of a vertical load of 7kN, defect-free FSP regions are produced irrespective of tool pin profiles. They also concluded that square pin profile produced defect-free welds irrespective of any vertical loads within their experimental domain (Elangovan et al. 2008). Rose et al. concluded the same, stating higher tensile properties for the moderate axial force with finer grain formation had achieved, whereas decreased tensile property is reported with both lower and higher amount of axial forces within their experimental domain (Rose et al. 2011). Several authors investigated newer tool design, and significant contribution has been marked by alterations of tool design in terms of improved material movement (Colegrove and Sherclliff 2005; Lorrain et al. 2010), enhanced microstructure

and mechanical properties (Elangovan and Balasubramanian 2008; Reza-E-Rabby and Reynolds 2014; Shi et al. 2015; Trimble et al. 2015). Trimble et al. attempted to investigate the tool forces for FSW of AA2024-T3. They measured the tool forces using rotating component dynamometer and developed a 3D finite element model for predicting the tool forces. They inferred that tool damage or pin breaking is more likely to occur at tool plunging period or initial tool transition due to a higher force variation (Trimble et al. 2012).

AA 6061-T6 is a precipitation-hardened aluminum alloy (Al–Mg–Si alloy) and possesses moderate strength with excellent corrosion resistance. It is extensively used for fabrication of lightweight structures, where a high strength-to-weight ratio and good corrosion resistance are requirements (Liu et al. 2013). Several researchers had shown their interest to analyze the effect of tool design and parametric alterations to assess heat transfer, material flow and mechanical properties. Rajakumar et al. (2011) in their study of effects of tool geometry reported that tool rotational speed and tool shoulder diameter were the most influential parameters for controlling mechanical properties as well as corrosion resistance. Hou et al. conducted experiments on AA 6061-T6 at constant welding speed to investigate the effect of rotational speed and varying bottom surface shoulder diameters for self-reacting friction stir welding. They concluded that with a lower diameter of bottom shoulder defective welds were produced with excessive flash, whereas increased rotational speed resulted in increased tensile properties initially with a remarkable decrease for a further increase due to the formation of void defects (Hou et al. 2014). He et al. investigated the effect of tool rotational speed on thick AA 6061-T6 plates. They concluded with increased tool rotational speed weld nugget grain size increases and the average microhardness encountered a decrease. The joints performed with 700 RPM (intermediate range) exhibits the highest tensile strength with a smooth residual stress distribution (He et al. 2016). Sun et al. studied the effect of the stationary shoulder on friction stir-welded AA6061-T6 for strength and toughness. They reported a significant weakening of strength and toughness in HAZ nearest to the

nugget zone. They concluded dissolution of β″ precipitates and re-precipitation of coarser 'β′ particles are associated with such degradation in HAZ (Sun et al. 2016). However, comparatively less research has been carried out to study the effectiveness of different tool designs from the perspective of torque and force analysis in this particular type of alloy. Threaded tools are believed to provide better weld qualities by improved material flow (Zhao et al. 2005). The present study is aimed to analyze the effectiveness of taper threaded tool in terms of spindle torque and force generation and their consequences on weld qualities at varying traverse speeds. For a better understanding of the results, a plain taper tool with similar dimension is incorporated in the study for comparative purpose.

2 Materials and Methods

AA 6061-T6 plates of 6 mm thickness in square butt configuration are used for this study. All the welding is conducted on a 3-ton friction stir welding setup. Two different types of tools viz. a taper (TT) and taper threaded (TTh) tool fabricated with H13 steel are used for this purpose (Fig. 2, Table 1). For this study, tool rotational speed is kept constant at 1100 RPM and traverse speed is varied in four levels (Table 1). From the literature, it is evident that at a lower

rotational speed less plastically deformed material is formed and at high rotational speed often the reverse is achieved. Both these conditions yield to the formation of a defect in weld nugget due to inappropriate material flow. To avoid such conditions, there is a requirement of selecting a suitable rotational speed within an intermediate range facilitating easy variation in traverse speed. Hence, tool rotational speed is kept constant at 1100 RPM on the basis of trial and error method. Spindle torque and different forces are measured using strain gauge based load cells. Two different load cells are used, one attached with spindle head (5 tones) for spindle torque and Z-force measurement and another load cell (3 tones) is attached with auxiliary slide for X-force measurement. These load cells are attached to the PLC system for data feedback, and NI LabView software is used for data acquisition. For a better understanding of the obtained results, weld thermal cycle is recorded using K-type thermocouple at a distance of 6 mm from the center of weld nugget. The macrostructure of the weld zone is analyzed using a light optical microscope. The grain size of weld nugget is analyzed using a light optical microscope. Average grain diameter is measured according to ASTM standard using the linear intercept method. Specimens for tensile testing were cut along the transverse to the weld direction and prepared according to ASTM-E8 standard. Tensile tests were carried out in INSTRON 8801 (strain rate-1 mm min^{-1}).

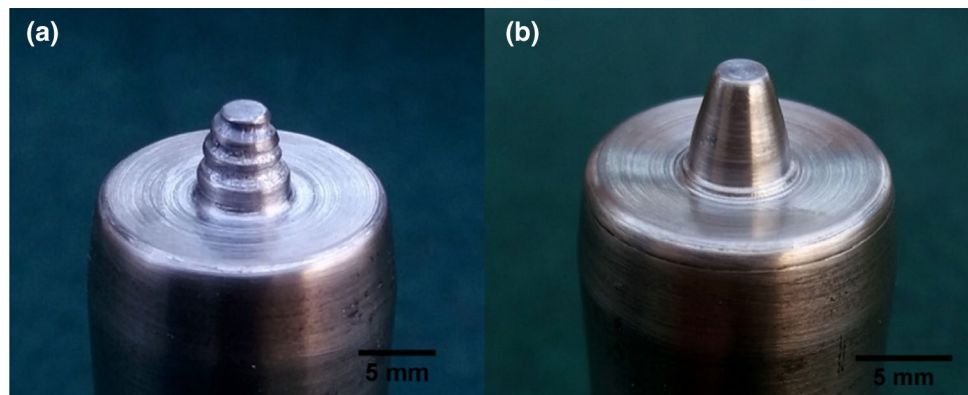**Fig. 2** Tool used in the present study **a** taper threaded (TTh), **b** taper (TT)

Table 1 Details of the workpiece, tool and process parameters

Material used	6061-T6
Plate dimension	150 mm×65 mm×6 mm with effective weld length of 120 mm
Material chemical composition (wt%)	Mg (1.2), Mn(0.15), Cu(0.2), Cr(0.04), Si(0.6), Fe(0.75), Al(Bal.)
Mechanical property	UTS-310 MPa, YS-276 MPa elongation—18%, hardness—107 (HV$_{0.1}$)
Tool shoulder diameter	18 mm
Tool pin bottom and top diameter	6 mm, 3 mm
Process parameters	Rotational speed—1100 RPM, traverse speed—45,75,105,135 mm/min, tilt angle—3°, plunge depth of shoulder—0.1 mm, dwell time—4 s

Fractography analysis of fractured samples is carried out using scanning electron microscope.

3 Results

3.1 Variation in Spindle Torque, Z-force and X-force

Figure 3a–c depicts the variation in spindle torque, downward vertical force (Z-force) and welding force (X-force), respectively, as welding proceeds for both TT and TTh tool. The requirement of spindle torque for TTh tool in comparison with TT tool is more as the effective area of interaction between tool and workpiece has increased by the thread surface for TTh tool (Fig. 3a). The spindle torque and Z-force attained for both the tools are faced with a sudden fluctuation

at the initial stage of tool traverse which gradually decreases and becomes stable as the as the welding proceeds. A gradual decrease in torque values is observed for TTh tool at higher traverse speeds of 105 mm/min and 135 mm/min (Fig. 3a), whereas a gradual increase is obvious for TT tool at higher traverse speeds of 105 mm/min. An abrupt fluctuation in spindle torque values is recorded as the traverse speed is further increased to 135 mm/min.

From the distribution of Z-force (Fig. 3b), it is noticed that at the lowest traverse speed of 45 mm/min initially, no sudden fluctuation occurs; rather a gradually increasing trend is more prominent for both the tools. The trend of a gradual rise in Z-force at a lower traverse speed is less for TT tool compared to TTh tool. With a further increase in traverse speed, both the tools show a sudden hike followed by a decrease in initial Z-force which with the further
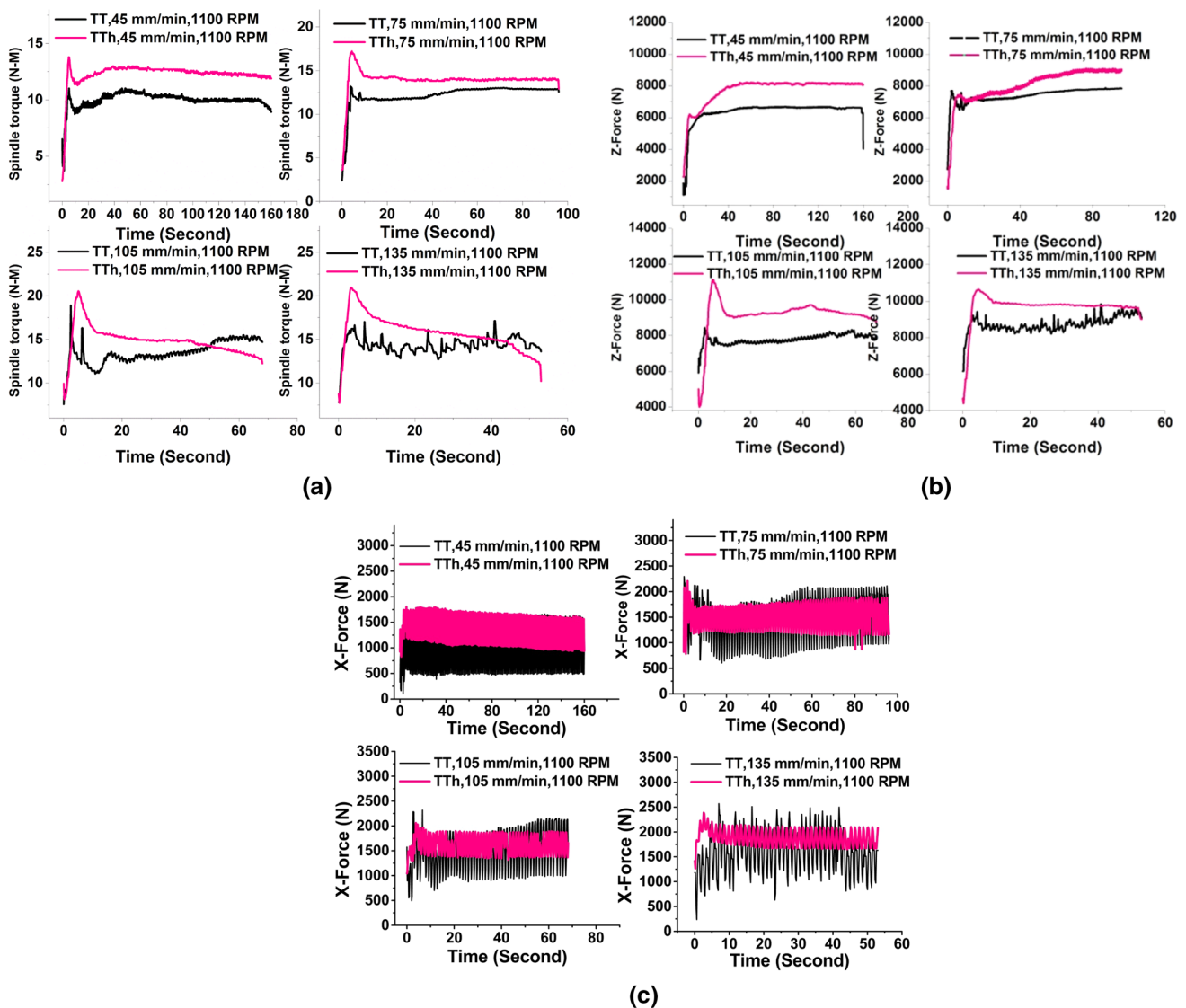

Fig. 3 Distribution of **a** Spindle torque, **b** Z-force, **c** X-force with time for TTH and TT tools with time for varying traverse speeds

Table 2 Average spindle torque, Z-force and X-force attained by taper (TT) and taper threaded (TTh) tool

Traverse speed (mm/min)	Spindle torque (N–M)		Z-force (N)		X-force (N)	
	TTh tool	TT tool	TTh tool	TT tool	TTh tool	TT tool
45	12.29	9.81	7740	6370	1351	1088
75	13.96	12.21	8031	7395	1540	1468
105	14.8	13.51	9156	7780	1620	1514
135	15.73	14.32	9667	8741	1880	1599

advancement of the tool stabilizes. But as tool traverses, Z-force gradually increases and at the highest traverse speed of 135 mm/min Z-force fluctuates severely for TT tool similar to that of spindle torque.

The distribution of X-force appears with a wider width due to the fluctuation of X-forces (Fig. 3c). The extent of fluctuation varies significantly for both tools. X-force distribution shows a higher fluctuation for TT tool compared to TTh tool. With the increase in traverse speed, the fluctuations for TT tool increases, whereas the trend marked is reverse for TTh tool. From Fig. 3c, it can be seen that with an increase in traverse speed from 75 to 105 mm/min X-force is less stable at initial transition period which stabilizes as welding proceeds for TT tool. With the further increase in traverse speed (135 mm/min) X-force loses its stability from initial transition period with irregular fluctuations which continue till the end of welding. No such observation is made for TTh tool at 135 mm/min. Another observation is that at a higher traverse speed the X-force fluctuation reduces, contrary to TT tool.

For both of the tools the average values of spindle torque, Z-force and X-forces increase with an increment in traverse speed. Higher values of all these entities are attained by TTh tool in comparison with TT tool (Table 2). The maximum torque, X-force and Z-force attained by the TTh tool are at 135 mm/min and are 15.73 N-m, 1880 n, 9667 n, respectively, whereas at 45 mm/min a minimum of 9.81 N-m, 1088 N and 6370 N are attained for torque, X-force and Z-force, respectively, by TT tool (Table 2).

3.2 Variations of Weld Thermal Cycle

The plots of weld thermal cycles are drawn to establish the differences of peak temperature attained by the tools. This is achieved at 6 mm away from the center of nugget in advancing side at a depth of 3.5 mm. With the increase in traverse speed, the period of thermal cycle decreases for the tools. Comparatively higher peak temperatures are achieved for TTh tool for all traverse speeds (Table 3, Fig. 4a, b). The presence of threads increases the effective surface area resulting in increased frictional heat, which contributes to increased peak temperature for TTh tool (Kadian and Biswas 2017; Sun and Wu 2018). The highest peak temperature attained by TT and TTh tool is 482.32 °C and 472.99 °C,

Table 3 Peak temperature attained for taper (TT) and taper threaded (TTh) tool with a variation in traverse speed

Traverse speed (mm/min)	Peak temperature (°C)	
	TTh tool	TT tool
45	482.32	472.99
75	471	459
105	443	429.21
135	402	381.31
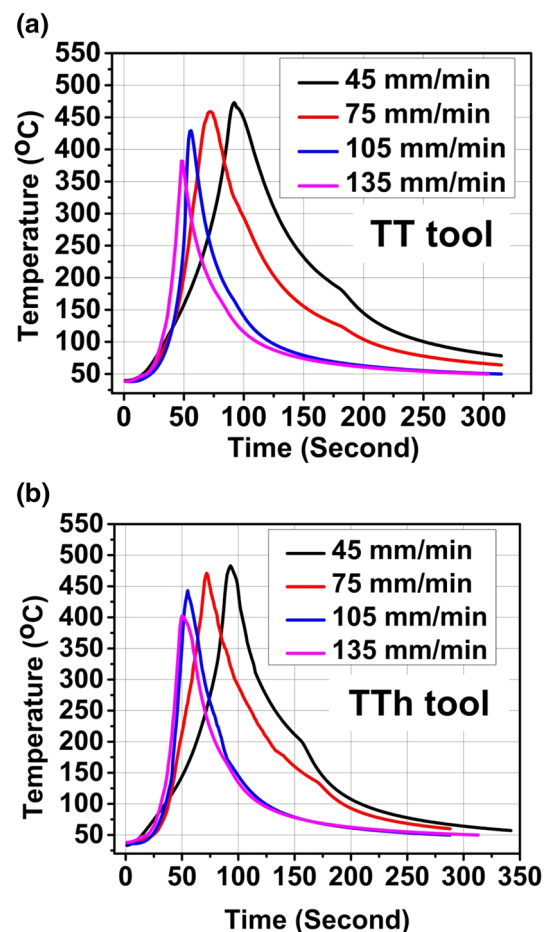
Fig. 4 Weld thermal cycle for **a** TT, **b** TTh tool with varying traverse speeds

respectively, at a traverse speed of 45 mm/min. Average values of torque, force and peak temperatures attained for both the tools are plotted in Fig. 5a, b for a comparative analysis of torque and forces and their behavior with peak temperature for varying traverse speeds. As traverse speed increases, a fall in peak temperature for the tools can be seen which is accompanied by an increase in spindle torque, X-force and Z-force.

3.3 Macrostructural Observation

Figure 6 represents the cross-sectional macrostructure of all the welding. Macrostructures for TTh tool reveal a stacked onion ring pattern for almost all samples, whereas no such pattern of onion ring is witnessed for TT tool. Area of weld nugget zone and thickness of shoulder influenced region are evaluated and represented in Fig. 7a, b. The thickness of shoulder influenced region is considered to be the distance from the top of weld nugget surface to the point

of intersection of the line drawn through the flow arm at advancing side and the weld nugget axis at center. A larger weld nugget area and thickness of shoulder induced region are more apparent for TTh tool than TT tool (Fig. 7a, b). With the increase in traverse speed from 45 to 75 mm/min the nugget area increases from 25.93 and 24.21 mm^2 to 49.12 and 41.6 mm^2 for TTh and TT tool, respectively. Further increase in traverse speed is encountered with a reduction in nugget area which is minimum at 135 mm/min with 37.93 and 34.46 mm^2 for TTh and TT tool, respectively. The same trend is true for the thickness of the shoulder induced region. A maximum thickness of 1.7 mm and 1.57 mm is attained by TTh and TT tool, respectively, at 75 mm/min which reduces further with traverse speed and is minimum at 135 mm/min with a thickness of 1.25 mm and 1.17 mm for TTh and TT tool, respectively.

3.4 Microstructural Observation

3.4.1 Grain Size Distribution

The distribution of nugget zone grain size reveals comparatively finer grains are attained by TTh tool (Fig. 8). The average grain diameter at the middle of the nugget is determined using linear intercept method according to ASTM E 112-12 (Fig. 9). Grain size is measured at three different locations at the center of the nugget, and the average value is considered. With the increase in traverse speed, the grain size decreases for both of the tools. For TTh tool at 135 mm/min, a finer grain size is obtained with an average grain diameter of 5.82 μm, whereas for TT tool a finer grain size with an average grain diameter of 8.68 μm is obtained at 135 mm/min.

3.4.2 Formation of Secondary Particles

Scanning electron micrographs of nugget zone taken in BSE mode (Fig. 10) shows mostly the formation of Mg_2Si particles which is the prime secondary phase formation for Al–Mg–Si alloys (AA 6061-T6). The pits and the small white marks represent the distribution of second phase particles. The pits have been formed around the second phase particles due to the corrosive action of the etching agent. The strengthening particles for TTh tool are finer and more uniformly distributed.

3.5 Mechanical Properties

3.5.1 Hardness

Evaluation of variation in Vickers hardness profile is one of the reliable methods for analyzing the microstructural changes for friction stir-welded aluminum alloys. It is measured along the horizontal line through the center of nugget
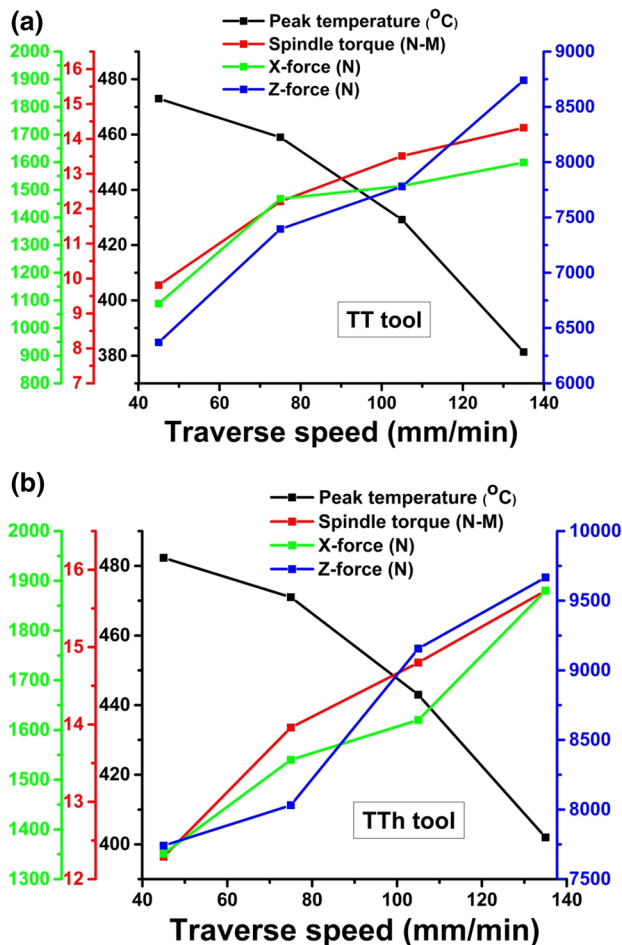

Fig. 5 Comparison of average spindle torque, Z-force and X-force with peak temperature for **a** TT tool, **b** TTh tool with varying traverse speeds
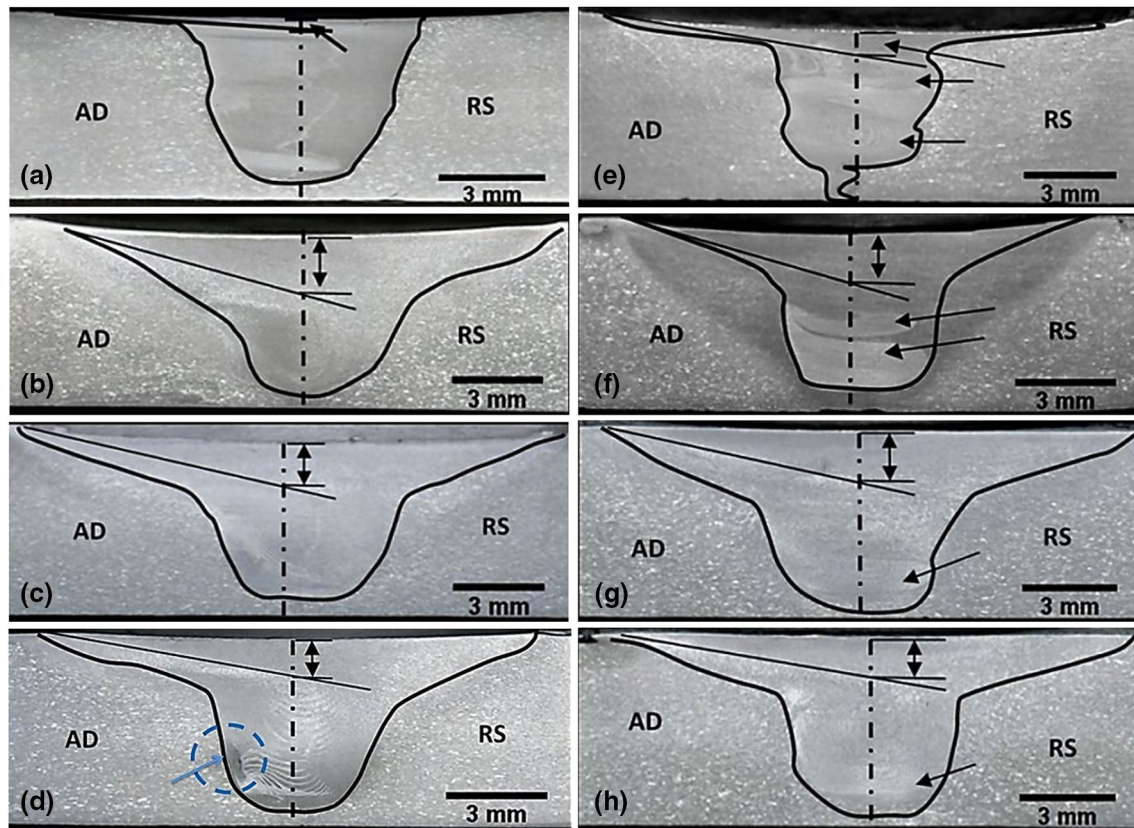
Fig. 6 Cross-sectional macrostructure of FSW weld for TT tool (traverse speed **a** 45 mm/min, **b** 75 mm/min, **c** 105 mm/min, **d** 135 mm/min. Cross-sectional macrostructure of FSW weld for TTh tool (traverse speed **e** 45 mm/min, **f** 75 mm/min, **g** 105 mm/min, **h** 135 mm/min)

(Fig. 11). The base metal hardness is around 107 HV. With the increase in traverse speeds, the hardness of the nugget zone for both tools increases. For all the welding, the TT tool exhibits higher hardness in nugget zone. The highest hardness achieved is around 79 HV and is attained for the taper tool at 135 mm/min in nugget zone. At the lowest traverse speed, the hardness achieved at nugget zone is around 70 HV and 60 HV for TT and TTh tool, respectively. At the highest traverse speed (135 mm/min), hardness achieved for TT and TTh tool is around 78 HV and 70 HV, respectively, whereas a shift of the lowest hardness point is witnessed for TTh tool at higher welding speeds (105,135 mm/min) from advancing side to retreating side.

3.5.2 Tensile Properties

Transverse tensile properties of friction stir-welded AA 6061-T6 for two different tools with varying traverse speeds are evaluated (Fig. 12). All the values are evaluated by averaging three results. From the figure, it can be ascertained that tool design and tool traverse speed have a distinct effect on tensile properties. TTh tool exhibits higher values of tensile property irrespective of all traverse speeds considered for

the study than TT tool. With the increase in traverse speed tensile properties increase for TTh tool, whereas for TT tool the tensile properties increase with traverse speed and attain highest values at 105 mm/min but with further increase in traverse speed at 135 mm/min it reduces to 176 MPa. The maximum tensile strength attained by the TT and TTh tool is 220 MPa and 187 MPa at 105 mm/min and 135 mm/min, respectively.

3.6 Fracture Type and Surface

Analysis of fracture samples and surface reveal a significant variation in fracture locations and failure mechanisms under tensile loading with a variation in traverse speed for both the tools (Fig. 13). The observations for the fractured sample are stated in Table 4. All the samples for TT tool failed at the advancing side weld beyond the nugget with a significant amount of deformation at fracture position, except the specimen welded at 135 mm/min (Fractured at the nugget). As evident from the macroscopic study of the fractured samples (Fig. 13a, c, e, g). At a lower traverse speed (45 mm/min, 75 mm/min and 105 mm/min), TT tool fracture surface is characterized with dimple shapes. This indicates the ductile
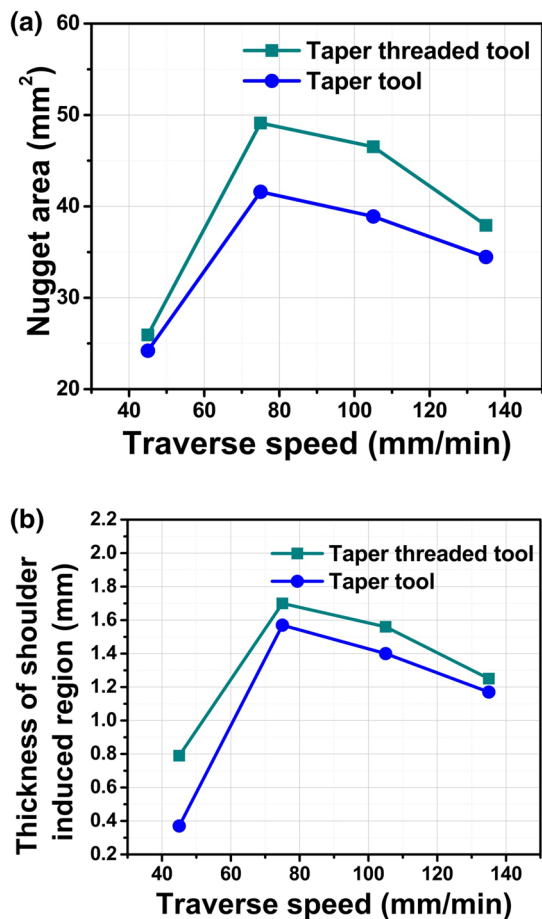
Fig. 7 a Variation in weld nugget area with the variation of traverse speed. **b** Variation in the thickness of shoulder induced region with the variation in traverse speed

mode of fracture has happened, whereas at a higher traverse speed (135 mm/min) for TT tool elongated and comparatively smaller dimples in cleavage form have been obtained. This indicates a mix mode of fracture with comparatively less yielding. But for TTh tool all the fractured samples are characterized with dimple formation indicating ductile failure even at a higher traverse speed (135 mm/min). For TT tool at the highest traverse speed (135 mm/min), the sample failed at nugget toward advancing side.

4 Discussion

4.1 Effect of Tool Design and Traverse Speed on Spindle Torque

Spindle torque is the material's response to resist the angular deformation imposed by the rotating tool. From the result section, it is evident that spindle torque varies distinctly with variation in both tool design and traverse speed (Fig. 3a).

As the tool proceeds through joining line, a higher interaction time (caused by a lower traverse speed) will lead to the generation of more heat (as evident from Fig. 4a, b). This eventually leads to the better deformation of the workpiece. Since the tool has to traverse across the less deformed material at higher traverse speeds (105 mm/min and 135 mm/min), a sudden hike in initial values of spindle torques is obtained (Fig. 3a). With further advancement of the tool, spindle torque decreases and comes to a stable position as joining line ahead of the tool may get sufficiently preheated. The area of interaction between tool pin and workpiece is less for TT tool compared to TTh tool due to the absence of threads. This causes generation of less frictional heat and further thread incorporated deformation is absent for TT tool. These factors when further associated with a comparatively higher traverse speed resulted in the requirement of enhanced torque for material deformation resulting in a gradual increase in spindle torque. The same analogy is valid for fluctuation of spindle torque for TT tool at 135 mm/min. This fluctuation reveals the inability of TT tool to stir the material effectively at a higher traverse speed indicating a sign of increased sliding condition between tool and workpiece interface. From Fig. 5a, b, it is clear that with the increase in peak temperature spindle torque and other forces decrease. This proves that a higher peak temperature which is a manifestation of increased heat input causes higher deformation (leading to higher plasticized material). As a result, less torque and forces are required to stir the deformed material.

4.2 Effect of Tool Design and Traverse Speed on Z-force and X-force

The downward material flow incorporated by tool pin is more for unit length due to a higher interaction time at lower traverse speeds. This results in the availability of less material under the shoulder causing a lesser hike in the initial Z-force and a gradual increase with time (Fig. 3b). At increased traverse speed, heat input decreases resulting in a decrease in downward flow and comparatively less deformed material available under the shoulder. It causes an initial hike in the Z-force value at higher traverse speed (105 mm/min and 135 mm/min) as well as increased Z-force (Fig. 3b). FSW is an asymmetrical welding process where the advancing and retreating sides exhibit a difference in heat generation and material flow (Kadian and Biswas 2017; Sun and Wu 2018). Typically, the advancing side of the weld attains higher heat generation where the shearing action is more prominent than the retreating side. All these phenomena create a difference in flow stress in advancing and retreating side and that can be sensed by the tool as a fluctuation of forces during rotation. At the higher traverse speed, since the
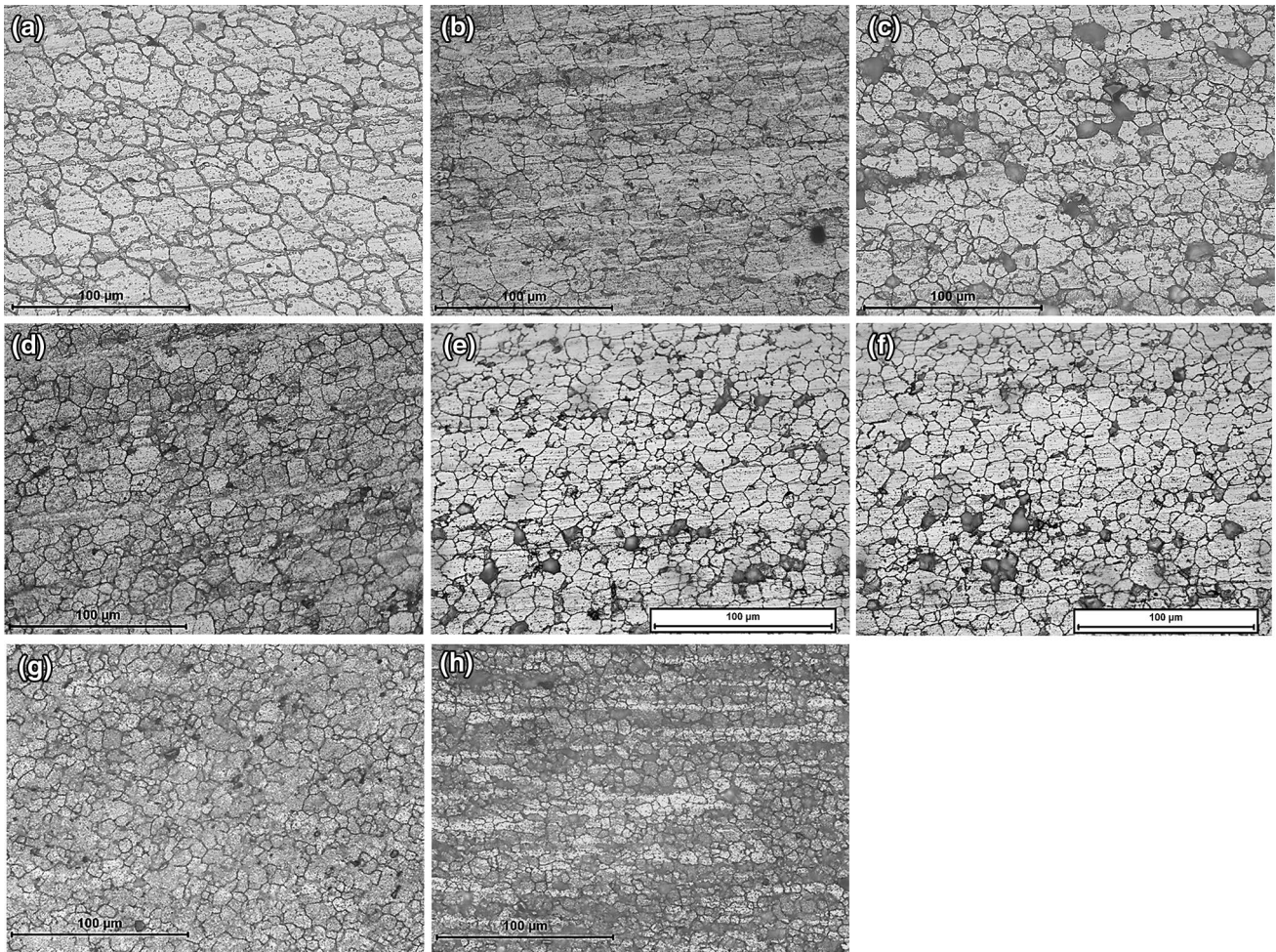
Fig. 8 Nugget zone grain size for TT tool (traverse speed **a** 45 mm/min, **b** 75 mm/min, **c** 105 mm/min, **d** 135 mm/min. Nugget zone grain size for TTh tool (traverse speed **e** 45 mm/min, **f** 75 mm/min, **g** 105 mm/min, **h** 135 mm/min)
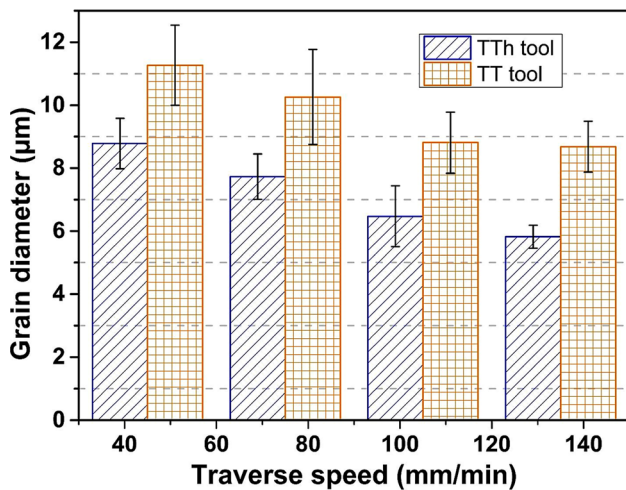

Fig. 9 Average grain diameter of nugget zone for both the tool with varying traverse speeds

heat input is less, much force is required to shear the less deformed material from advancing side. Moreover, it has to pass through the retreating side with less force (since the shearing action is less). This causes a larger drop in forces causing a higher fluctuation which is evident from Fig. 3b for TT tool at 135 mm/min. This may create a discontinuity and non-uniformity of material flow beneath the shoulder from advancing side to retreating side, causing instability in material movement. This indicates material flow under shoulder at higher traverse speed is less stable for TT tool, whereas no such increased fluctuation is detected for TTh tool since the larger area of threads generate more heat and a higher deformed material is available for TTh tool. Increased Z-force is a requirement to consolidate the less deformed material instigating a larger Z-force at a higher traverse speed. The same analogy is justified for increased X-force for increased traverse speed. As depicted in Fig. 3c, an abrupt behavior of X-force with irregular fluctuation depicts the inability
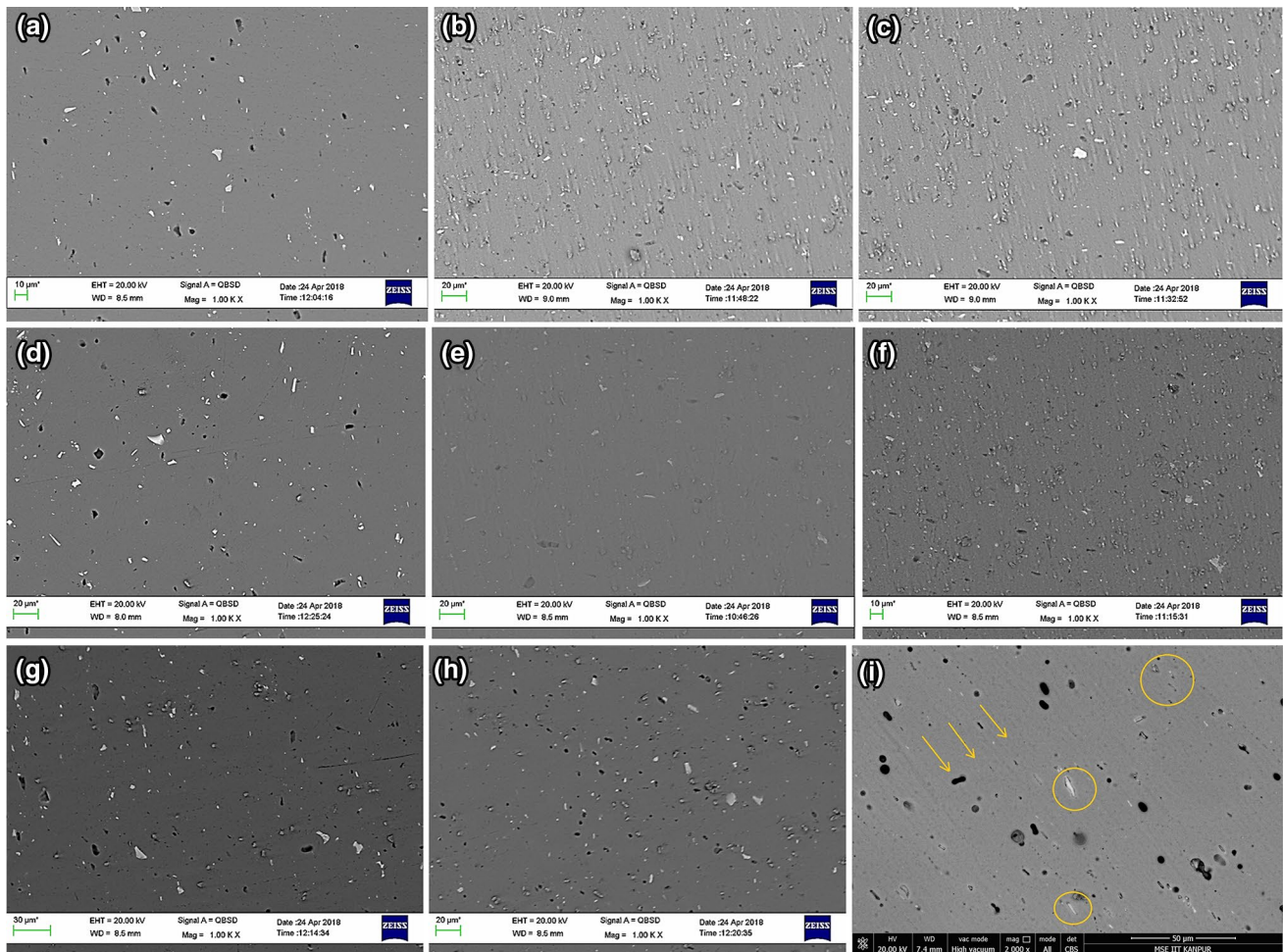
Fig. 10 SEM image of secondary particle distribution for TT tool (Traverse speed **a** 45 mm/min, **b** 75 mm/min, **c** 105 mm/min, **d** 135 mm/min. SEM image of secondary particle distribution for TTh tool (traverse speed **e** 45 mm/min, **f** 75 mm/min, **g** 105 mm/min, **h** 135 mm/min). **i** SEM image of secondary particle distribution for base material (AA 6061-T6)

of TT tool to maintain a better material movement at increased traverse speed (135 mm/min), whereas comparatively more stable X-force distribution is achieved for TTh tool for all cases. This clearly shows that TTh tool manages the material flow more effectively even though the average X-force for TTh tool is comparatively higher (Fig. 4b). All these together led to the observation of reduced X-force fluctuation even at increased traverse speed for TTh tool contrary to TT tool. Such decrease in X-force fluctuation is an indication that even at a higher traverse speed TTh tool is capable of providing better material movement compared to TT tool. This difference can be attributed to the thread incorporated feature of TTh tool. For TT tool, both Z-force and X-force are comparatively less than TTh tool as the amount of material deformed has increased due to the larger surface area of TTh pin.

4.3 Analysis of Macrostructural Property

As the tool rotates and traverses it forces the material of leading side of the tool pin and displaces it to the trailing side over the pin surface resulting in the formation of nugget zone (Mehdi and Mishra 2018). Material flow under the shoulder is commonly known as shoulder induced flow. It is governed by the forging action of the shoulder and shearing of material in advancing side by means of applied vertical force and shoulder rotation. The increased tool–workpiece interaction area caused by threads in TTh tool leads to the observation of larger weld area (Fig. 7a, b). Moreover, the requirement of increased torque and Z-force contributes to the increased amount of material deformation leading to larger weld zone (Figs. 6, 7). Larger vertical forces (Z-force) attained by TTh tool contribute to the better consolidation of deformed material behind the tool. Moreover, the fluctuations in material
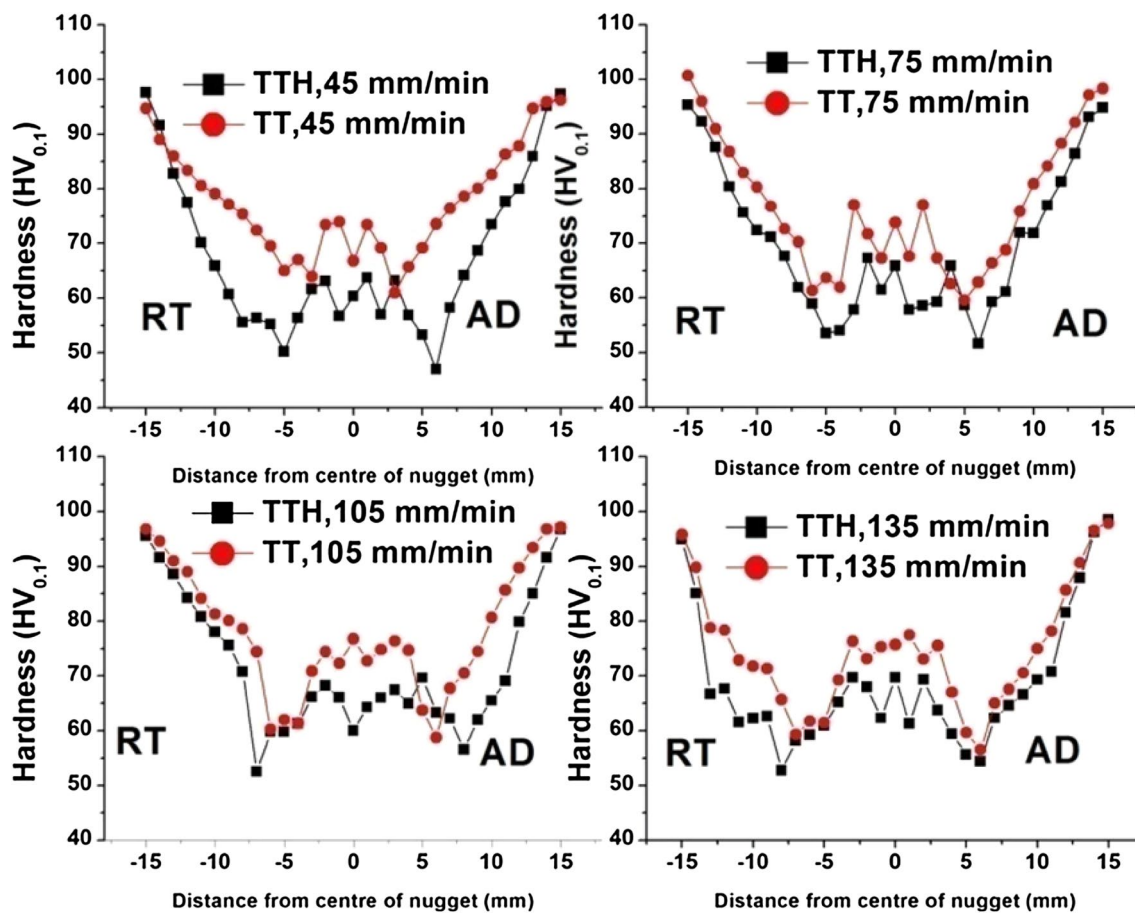
Fig. 11 Microhardness profile across along the center of nugget in horizontal direction

flow resistance (X-force) experienced by the tool pin is more stable (Fig. 3c). The threads facilitate better downward material flow that indicates a balanced interaction between

Fig. 12 Variation in different tensile properties for taper (TT) and taper threaded (TTh) tool with a variation in traverse speed

shoulder and pin induced flow in case of TTh tool. All these factors contribute to the better consolidation of displaced material by the shoulder. This led to the observation of comparatively thicker shoulder induced region for TTh tool and a uniform material flow in nugget. Increased traverse speed leads to a less plasticized material; hence, the requirement of a larger vertical force arises (Fig. 3b). Moreover, material flow resistance (X-force) increases with traverse speed (Fig. 3c, 4). This indicates that downward flow decreases for increased traverse speed resulting in a reduction in thickness of shoulder induced region. However, increased plasticization at lower traverse speed (45 mm/min) assists in increased sliding condition resulting in the reduction in thickness of shoulder induced region. A poor material flow is achieved as evident from the distribution of abrupt changes in torque and forces (Fig. 3a–c) at 135 mm/min. This forms a tunnel defect at the advancing side of nugget-TMAZ interface for TT tool, whereas no such defects can be seen for TTh tool due to thread-guided flow. Moreover, for TTh tool a stacked layered onion ring pattern is obtained, whereas for TT tool no such observation can be confirmed (Fig. 6). This stacked layered onion ring pattern may be obtained due to
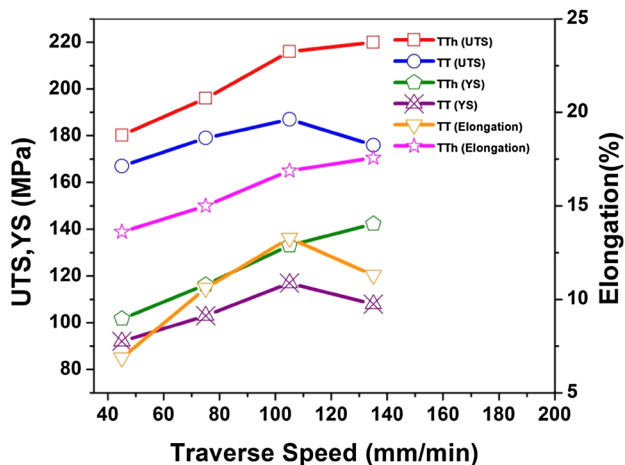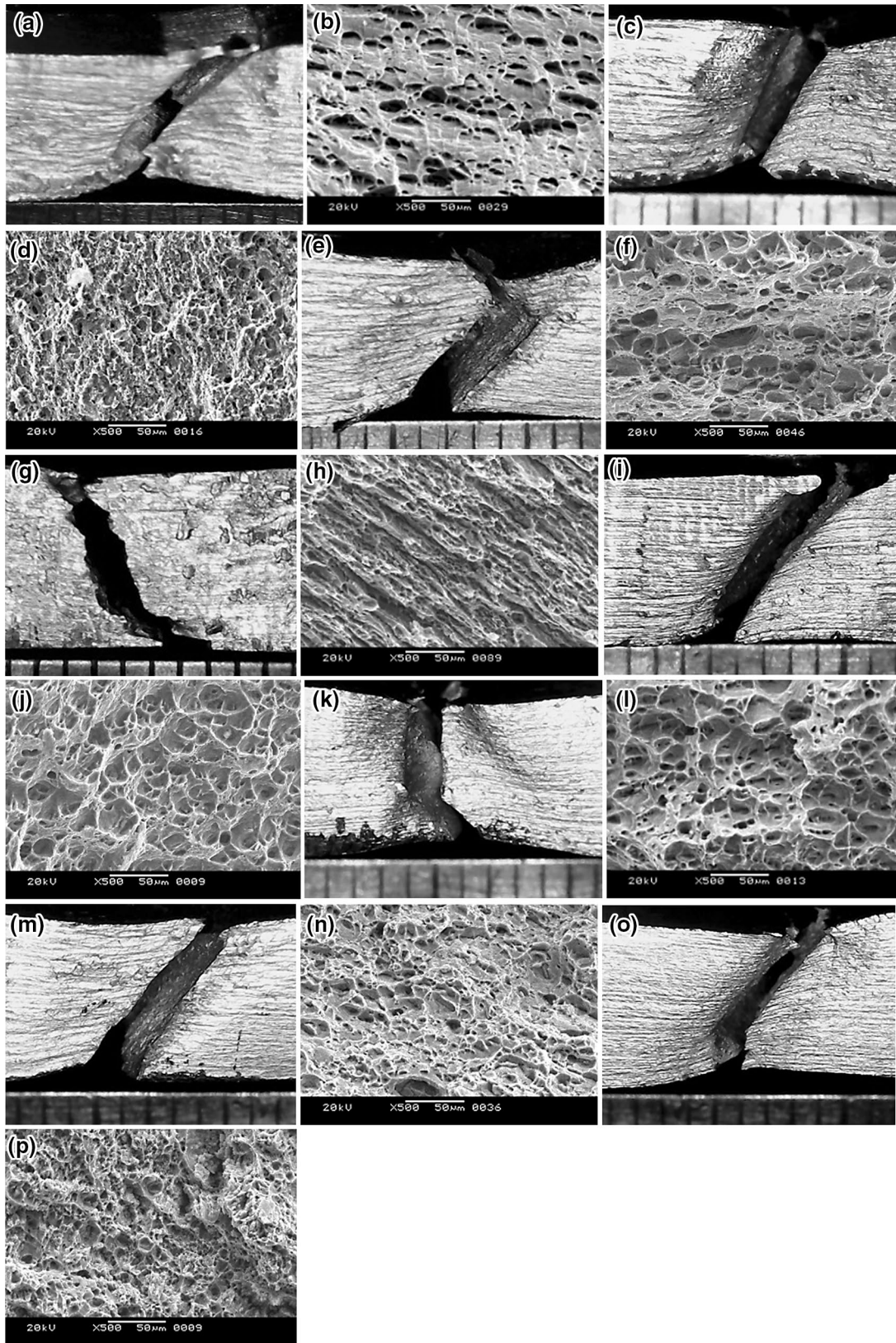
Fig. 13 Variation of fracture type and surface respectively for taper tool (TT) with varying traverse speeds (**a**, **b** 45 mm/min, **c**, **d** 75 mm/min, **e**, **f** 105 mm/min, **g**,**h** 135 mm/min) and for taper threaded tool (TTh) (**i**, **j** 45 mm/min, **k**, **l** 75 mm/min, **m**, **n** 105 mm/min, **o**, **p** 135 mm/min)

Table 4 Variation in fracture type for taper (TT) and taper threaded (TTh) tool with a variation in traverse speed

Traverse speed (mm/min)	Taper tool (TT)	Taper threaded tool (TTh)
45	Coarse elongated dimples Fracture position—at advancing side, outside nugget fracture type—ductile	Coarse dimples Fracture position—At advancing side, outside nugget Fracture type—ductile
75	Small dimples shape with layered morphologies Fracture position—at advancing side, outside nugget Fracture type—mix mode of failure	Coarse dimples Fracture position—at advancing side, outside nugget Fracture type—ductile
105	Coarse dimples Fracture position—at advancing side, outside nugget Fracture type—ductile	Fine dimples Fracture position—At retreating side, outside nugget Fracture type—ductile
135	Elongated cleavage surface Fracture position—from the bottom of nugget (at weld center) toward advancing side Fracture type—mix mode of failure	Very fine dimples Fracture position—at retreating side, out side nugget Fracture type—ductile

the influence of thread-induced flow. The presence of this stacked multiple onion rings is an indication of the formation of multiple localized flow around the threaded pin which facilitates better material mixing.

4.4 Analysis of Microstructural Property

Due to dynamic recrystallization, equiaxed grains are observed in the nugget zone for all the welding (Fig. 8). Grain size in friction stir welding depends on different factors such as heat input, cooling rate and the extent of deformation. Higher heat input results in better deformation of the workpiece. Aluminum alloys are susceptible to grain growth at a lower cooling rate which provides a higher nucleation time (Attallah and Salem 2005). Also, a higher heat input assists more intense deformation which yields finer grains. However, faster removal of heat from the weld zone is also a concern to avoid any grain growth assisted by increased nucleation time due to a lower cooling rate. Largely it has seen that a higher heat input is associated with grain growth for FSW of aluminum alloy since it is a comparatively slower welding process where heat source (tool) moves slowly (Attallah and Salem 2005; Mishra and Ma 2005). With the increase in traverse speed, grain size becomes finer for both the tools since heat input decreases due to less interaction time. Also, from the weld thermal plot of the weld zone, it can be seen that faster traverse speed ensures faster cooling due to increased heat source speed, thus reducing grain nucleation time. TTh tool exhibits finer grains compared to TT tool due to a higher heat input which assists better plasticization and is further complimented by threads present in the TTh tool (Fig. 9).

From Fig. 10i, it can be observed that the secondary particles for the base material are coarser (elongated) and oriented in the rolling direction. In friction stirred samples, the strengthening particles mostly get dissolved into nugget

zone due to high heat input as well as high strain rates during welding. However, depending on various conditions re-precipitation and coarsening of those second phase particles may happen in the nugget zone. At a lower traverse speed, the heat input and tool stirring time cause more dissolution of second phase particles, which decreases at increased traverse speeds. With the increase in traverse speeds the amount of strengthening particles increases for both of the tools. The higher amount of Spindle torque, Z-force and lower fluctuation of X-forces improved the stirring action and material flow for TTh tool. This assists the strengthening particles to break down in finer mode.

4.5 Analysis of Hardness

Comparatively higher hardness is achieved for TT tool than TTh tool beside the fact that TTh tool exhibits a finer grain size (Fig. 11). Such behavior can be attributed to the fact that the properties of precipitation-hardened aluminum alloy, like AA 6061-T6, largely depend on the formation and distribution of second phase precipitates in addition to grain size. As discussed earlier, higher deformation and heat input attained by TTh tool leads to the dissolution of second phase precipitates. This causes softening of nugget zone. Increasing the mechanical properties by means of achieving fine recrystallized grain is always a concern for researchers in the field of friction stir welding. Ahemdenia et al. (2015) found that increased power of ultrasonic-assisted friction stir welding provides finer recrystallized grains which in turn improves the microhardness property of stir zone by 10 HV. Zhou et al. reported that at higher RPM comparatively coarser grains and precipitation phase was obtained due to longer duration of weld thermal cycle. As an effect, the hardness of weldment decreases (Zhou et al. 2017). With the increase in traverse speeds, the hardness for both tools increases and this may be attributed to the formation of finer grain size and

fine particle distribution in nugget zone. The hike of hardness values in nugget zone for TTh tool is more (60 HV to 70 HV) with the increase in traverse speed in comparison with TT tool (78 HV and 70 HV). This is also an indication that at lower traverse speeds the dissolution of second phase precipitates is comparatively more for TTh tool than TT tool as evident from Fig. 10a, e. The lowest hardness point is achieved at the advancing side for TT tool. It is due to the fact that more heat is produced at advancing side of the welding as the tool has to shear the material from advancing side which may cause grain growth and precipitate dissolution in advancing side for TT tool, whereas the lowest hardness point changes to retreating side in case of TTh tool at higher welding speeds (105 mm/min and 135 mm/min). As at higher traverse speed heat input is less, thread incorporated shearing action is more on less deformed material on retreating side. Higher amount of torque and forces are also encountered by the workpiece. Such circumstances may cause comparatively enhanced grain elongation in retreating side causing such reduction in hardness.

4.6 Analysis of Tensile Strength and Fractography

From the result section, it is inferred that higher tensile properties of the welded joint are obtained for TTh tool compared to that for TT tool (Fig. 12). Higher vertical forces and torque attained by TTh tool (Fig. 3a, b) leads to better management of plasticized material flow and contributes to the formation of finer grains by means of higher deformation (Figs. 8, 9). According to Hall–Petch relationship, finer grain size results in improved tensile strength (Hall 1954; Mironov et al. 2014). Higher torque and force assist in breaking down of strengthening particles to a finer level (Fig. 10). All these factors contribute to a more uniform and fine distribution of strengthening particles for TTh tool leading to enhanced tensile properties, whereas a sudden decrease in tensile properties for TT tool at a traverse speed of 135 mm/min is marked and is attributed to the formation of tunnel defect (Figs. 6, 14). The fractography study of fractured tensile sample also supports this observation. From Fig. 13g, it is revealed that the fracture is roughly taking place at the tool pin and workpiece interface in nugget zone through the tunnel formation (Fig. 6d). Also, the deformation in the macroscopic level is much less. This indicates poor bonding is taking place in the nugget, due to increased sliding condition at a higher traverse speed. At a lower traverse speed (45 mm/min and 75 mm/min), for TTh tool the fracture occurs at advancing side. This is a regular observation since the higher temperature is attained by the advancing side and this may lead to grain growth, causing the lowest hardness region. But with the increase in traverse speed (105 mm/min and 135 mm/min) the fracture position shifts from advancing to
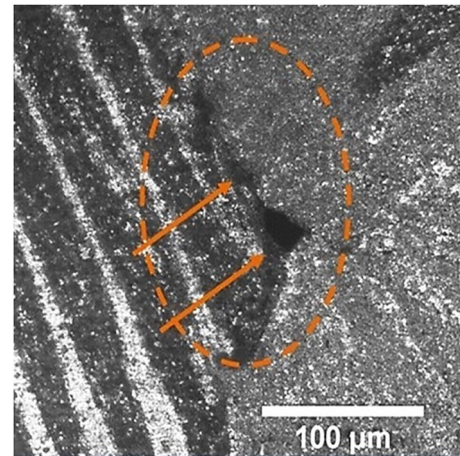

Fig. 14 Defect formation for TT tool at 135 mm/min

the retreating side for TTh tool. This happens as the lowest hardness point shifts to the retreating side for TTh tool.

5 Conclusion

The present study aimed at the experimental investigation of the effect of threaded tool pin feature on spindle torque and force variation and their effect on microstructure and mechanical properties. The conclusions that can be drawn from the analysis are listed below:

- With the increase in traverse speed spindle torque, X-force and Z-force increase for both tools. Comparatively higher values of these entities are attained by taper threaded tool (TTh).
- A maximum torque, X-force and Z-force are attained by the TTh tool at 45 mm/min and are 15.73 N-m, 1880 N, 9667 N, respectively, whereas the minimum of these entities was attained by TT tool at 45 mm/min and are 9.81 N-M, 1088 N, 6370 N, respectively.
- With the increase in traverse speed, the fluctuation of X-force reduces for TTh tool, converse to TT tool.
- The peak temperature increases for both tools with a decrease in traverse speed. The TTh tool attains the highest peak temperatures irrespective of traverse speed. The highest peak temperature attained by TT and TTh tool is at 45 mm/min and is 482.32 °C and 472.99 °C, respectively.
- The area of weld nugget and thickness of shoulder influenced region is more for TTh tool irrespective of traverse speed. A lowest weld nugget area and thickness of shoulder induced region is obtained for TT tool at 45 mm/min and are 24.21 mm^2, 0.37 mm, respectively, whereas at

75 mm/min the maximum of these entities is encountered for TTh tool and is 49.12 mm^2 and 1.57 mm, respectively.

- Onion ring patterns are prominent at a lower traverse speed for TTh tool, whereas for TT tool they are more prominent with a higher traverse speed. Vertically stacked incomplete half elliptical shaped onion rings are achieved by TTh tool.

- Finer grain size and strengthening precipitates with uniform distribution are observed for the TTh tool. With the increase in traverse speed, grain size becomes finer for both the tools, whereas at a lower traverse speeds the strengthening particles are more dissolved. At 135 mm/min, the TTh tool exhibits comparatively finer grain size with an average grain size of 5.82 μm.

- The tensile property increases for both of the tools with an increase in traverse speed. The maximum tensile strength attained by TT tool is at 105 mm/min (187 MPa), whereas maximum tensile strength for TTh tool is 220 MPa at 135 mm/min. At 135 mm/min, a sudden drop in tensile property is observed for TT tool to a value of 176 MPa.

References

Ahmadnia M, Seidanloo A, Teimouri R, Rostamiyan Y, Titrashi KG (2015) Determining influence of ultrasonic-assisted friction stir welding parameters on mechanical and tribological properties of {AA}6061 joints. Int J Adv Manuf Technol 78(9–12):2009–2024. https://doi.org/10.1007/s00170-015-6784-0

Attallah MM, Salem HG (2005) Friction stir welding parameters: a tool for controlling abnormal grain growth during subsequent heat treatment. Mater Sci Eng A 391(1–2):51–59. https://doi.org/10.1016/j.msea.2004.08.059

Banik A, Saha Roy B, Deb Barma J, Saha SC (2018) An experimental investigation of torque and force generation for varying tool tilt angles and their effects on microstructure and mechanical properties: friction stir welding of AA 6061-T6. J Manuf Process 31:395–404. https://doi.org/10.1016/j.jmapro.2017.11.030

Colegrove PA, Shercliff HR (2005) 3-Dimensional CFD modelling of flow round a threaded friction stir welding tool profile. J Mater Process Technol 169(2):320–327. https://doi.org/10.1016/j.jmatprotec.2005.03.015

Elangovan K, Balasubramanian V (2008) Influences of tool pin profile and welding speed on the formation of friction stir processing zone in {AA}2219 aluminium alloy. J Mater Process Technol 200(1–3):163–175. https://doi.org/10.1016/j.jmatprotec.2007.09.019

Elangovan K, Balasubramanian V, Valliappan M (2008) Influences of tool pin profile and axial force on the formation of friction stir processing zone in AA6061 aluminium alloy. Int J Adv Manuf Technol 38(3–4):285–295. https://doi.org/10.1007/s00170-007-1100-2

Hall EO (1954) Variation of hardness of metals with grain size. Nature 173(4411):948–949. https://doi.org/10.1038/173948b0

He J, Ling Z, Li H (2016) Effect of tool rotational speed on residual stress, microstructure, and tensile properties of friction stir welded 6061-T6 aluminum alloy thick plate. Int J Adv Manuf Technol 84(9):1953–1961. https://doi.org/10.1007/s00170-015-7859-7

Hou JC, Liu HJ, Zhao YQ (2014) Influences of rotation speed on microstructures and mechanical properties of 6061-T6 aluminum alloy joints fabricated by self-reacting friction stir welding tool. Int J Adv Manuf Technol 73(5–8):1073–1079. https://doi.org/10.1007/s00170-014-5857-9

Kadian AK, Biswas P (2017) Effect of tool pin profile on the material flow characteristics of {AA}6061. J Manuf Process 26:382–392. https://doi.org/10.1016/j.jmapro.2017.03.005

Kumar S (2016) Ultrasonic assisted friction stir processing of 6063 aluminum alloy. Arch Civ Mech Eng 16(3):473–484. https://doi.org/10.1016/j.acme.2016.03.002

Liu HJ, Hou JC, Guo H (2013) Effect of welding speed on microstructure and mechanical properties of self-reacting friction stir welded 6061-T6 aluminum alloy. Mater Des 50:872–878. https://doi.org/10.1016/j.matdes.2013.03.105

Lorrain O, Favier V, Zahrouni H, Lawrjaniec D (2010) Understanding the material flow path of friction stir welding process using unthreaded tools. J Mater Process Technol 210(4):603–609. https://doi.org/10.1016/j.jmatprotec.2009.11.005

Mehdi H, Mishra RS (2018) Analysis of material flow and heat transfer in reverse dual rotation friction stir welding: a review. Int J Steel Struct 1:13. https://doi.org/10.1007/s13296-018-0131-x

Mironov S, Inagaki K, Sato YS, Kokawa H (2014) Effect of welding temperature on microstructure of friction-stir welded aluminum alloy 1050. Metall Mater Trans A 46(2):783–790. https://doi.org/10.1007/s11661-014-2651-0

Mishra RS, Ma ZY (2005) Friction stir welding and processing. Mater Sci Eng R Rep 50(1–2):1–78. https://doi.org/10.1016/j.mser.2005.07.001

Rajakumar S, Muralidharan C, Balasubramanian V (2011) Predicting tensile strength, hardness and corrosion rate of friction stir welded {AA}6061-T6 aluminium alloy joints. Mater Des 32(5):2878–2890. https://doi.org/10.1016/j.matdes.2010.12.025

Reza-E-Rabby M, Reynolds AP (2014) Effect of tool pin thread forms on friction stir weldability of different aluminum alloys. Procedia Eng 90:637–642. https://doi.org/10.1016/j.proeng.2014.11.784

Rose AR, Manisekar K, Balasubramanian V (2011) Effect of axial force on microstructure and tensile properties of friction stir welded {AZ}61A magnesium alloy. Trans Nonferr Met Soc China 21(5):974–984. https://doi.org/10.1016/s1003-6326(11)60809-1

Santochi M, Dini G (1998) Sensor technology in assembly systems. CIRP Ann 47(2):503–524. https://doi.org/10.1016/S0007-8506(07)63239-9

Shi L, Wu CS, Liu HJ (2015) The effect of the welding parameters and tool size on the thermal process and tool torque in reverse dual-rotation friction stir welding. Int J Mach Tools Manuf 91:1–11. https://doi.org/10.1016/j.ijmachtools.2015.01.004

Sun Z, Wu CS (2018) A numerical model of pin thread effect on material flow and heat generation in shear layer during friction stir welding. J Manuf Process 36:10–21. https://doi.org/10.1016/j.jmapro.2018.09.021

Sun Z, Yang X, Li D, Cui L (2016) The local strength and toughness for stationary shoulder friction stir weld on {AA}6061-T6 alloy. Mater Charact 111:114–121. https://doi.org/10.1016/j.matchar.2015.11.020

Teti R, Jemielniak K, O'Donnell G, Dornfeld D (2010) Advanced monitoring of machining operations. CIRP Ann 59(2):717–739. https://doi.org/10.1016/j.cirp.2010.05.010

Thomas WM, Nicholas ED, Needham JC, Murch MG, Templesmith P, Dawes CJ (1991) GB Patent application no. 9125978.8. International Patent Application No. PCT/GB92/02203

Trimble D, Monaghan J, O'Donnell GE (2012) Force generation during friction stir welding of AA2024-T3. CIRP Ann 61(1):9–12. https://doi.org/10.1016/j.cirp.2012.03.024

Trimble D, O'Donnell GE, Monaghan J (2015) Characterisation of tool shape and rotational speed for increased speed during friction stir

welding of {AA}2024-T3. J Manuf Process 17:141–150. https://doi.org/10.1016/j.jmapro.2014.08.007

Yang Y, Kalya P, Landers RG, Krishnamurthy K (2008) Automatic gap detection in friction stir butt welding operations. Int J Mach Tools Manuf 48(10):1161–1169. https://doi.org/10.1016/j.ijmachtools.2008.01.007

Zhao Y, Lin S, Wu L, Qu F (2005) The influence of pin geometry on bonding and mechanical properties in friction stir weld 2014 Al alloy. Mater Lett 59(23):2948–2952

Zhou L, Luo LY, Zhang TP, He WX, Huang YX, Feng JC (2017) Effect of rotation speed on microstructure and mechanical properties of refill friction stir spot welded 6061-T6 aluminum alloy. Int J Adv Manuf Technol 92(9–12):3425–3433. https://doi.org/10.1007/s00170-017-0359-1